ACS Photonics

Letter

pubs.acs.org/journal/apchd5

Nonlinear Anisotropic Dielectric Metasurfaces for Ultrafast Nanophotonics

Giuseppe Della Valle,*[,†] Ben Hopkins,[‡] Lucia Ganzer,[†] Tatjana Stoll,[†] Mohsen Rahmani,[‡] Stefano Longhi,[†] Yuri S. Kivshar,[‡] Costantino De Angelis,[§] Dragomir N. Neshev,*[,‡] and Giulio Cerullo[†]

[†]Dipartimento di Fisica, Politecnico di Milano, and Istituto di Fotonica e Nanotecnologie del Consiglio Nazionale delle Ricerche, Piazza Leonardo da Vinci 32, 20133 Milano, Italy

[‡]Nonlinear Physics Centre, Research School of Physics and Engineering, The Australian National University, Canberra, ACT 2601, Australia

[§]CNISM and Dipartimento di Ingegneria dell'Informazione, Universitá di Brescia, Via Branze 38, 25123 Brescia, Italy

S *Supporting Information*

ABSTRACT: We report on the broadband transient optical response of anisotropic, amorphous silicon nanobricks that exhibit Mie-type resonances. A quantitative model is developed to identify and disentangle the three physical processes that govern the ultrafast changes of the nanobrick optical properties, namely, two-photon absorption, free-carrier relaxation, and lattice heating. We reveal a set of operating windows where ultrafast all-optical modulation of transmission is achieved with full return to zero in 20 ps. This is made possible because of the distinct dispersive features exhibited by the competing nonlinear processes in transmission and despite the slow (nanosecond) internal lattice dynamics. The observed ultrafast switching behavior can be independently engineered for both orthogonal polarizations using the large anisotropy of nanobricks, thus allowing ultrafast anisotropy control. Our results categorically ascertain the potential of all-dielectric resonant nanophotonics as a platform for ultrafast optical devices and reveal the possibility for ultrafast polarization-multiplexed displays and polarization rotators.

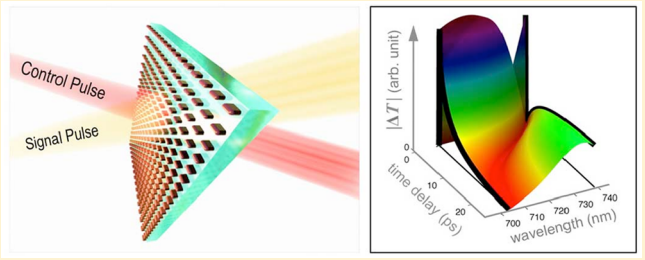

KEYWORDS: *Mie resonances, dielectric metasurfaces, Nonlinear optics, ultrafast spectroscopy, all-optical modulation*

Following the growth of nanofabrication technologies, there has been a burgeoning interest in periodic arrangements of resonant nanostructures, tightly packed as *meta-atoms*, which can form synthetic two-dimensional materials, or *metasurfaces*. These have enabled a host of novel applications for flat optics[1,2] and are now poised also toward nonlinear optical functionality.[3] The first meta-atoms utilized plasmonic resonances in noble metals, which also possess a strong optical nonlinearity.[4,5] The emergent vision was to exploit the nonlinearity in such plasmonic meta-atoms as a new route for all-optical modulation and switching and, more generally, for ultrafast nanophotonics.[6−15] However, the most eligible plasmonic metals exhibit very high linear and nonlinear ohmic losses, intrinsically related to the localized fields in a plasmonic resonance,[16] and are only weakly compatible with the large-scale CMOS integration platform.[17] The search for better plasmonic materials with lower losses remains a current and growing topic of interest,[18] where heavily doped semiconductors[19,20] and graphene[21] are good new candidates.

All-dielectric nanoresonators present an alternate route for nonlinear nanophotonics by exploiting Mie-type resonances instead of plasmonics. High refractive index dielectrics offer high-quality, localized resonances that can enable access to nonlinear functionalities while maintaining minimal ohmic losses.[22,23] Silicon has been the material of choice for nonlinear dielectric nanoresonators[24−26] offering strong nonlinear response and two-photon absorption (TPA).[27] Proof-of-principle attosecond experiments on silicon-based dielectrics also indicate the viability of extreme switching speeds with a bandwidth up to petahertz.[28,29]

Recently, all-optical switching in a planar array of hydrogenated amorphous silicon (a-Si:H) nanoresonators has also been demonstrated, exploiting Mie-like magnetic[30,31] and Fano resonances.[25] The observed all-optical modulation was found to be a result of the combined action of instantaneous TPA, free carrier generation, and thermal effects. However, despite the observed ultrafast dynamics, only modulation at a single wavelength and a single polarization has been measured, thus missing a plethora of opportunities for ultrafast spectral and polarization control. Furthermore, the interplay of the underlying physical mechanisms for optical modulation was never addressed, leaving it unclear as to what control is available over the transient dynamics.

Received: May 30, 2017
Published: August 16, 2017

DOI: 10.1021/acsphotonics.7b00544
ACS Photonics 2017, 4, 2129−2136

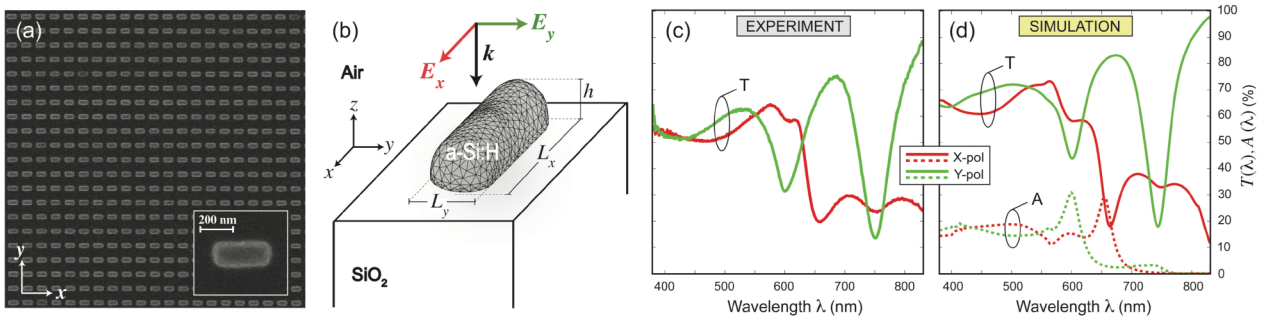

Figure 1. (a) SEM image of the dielectric metasurface made of a densely packed 2D array of a-Si:H nanobricks. (b) Sketch of the unit cell considered in the numerical simulations, showing the tetrahedral mesh employed to discretize the a-Si:H meta-atom. The incoming beam is modeled as a plane wave impinging at normal incidence, and two different linear polarizations are considered, with the electric field along the *x*-axis (red) or along the *y*-axis (green). (c, d) Transmission spectra of the anisotropic metasurface according to (c) experiments and (d) simulations (shared vertical axis). Dotted lines in (d) show the simulated absorption spectra.

Even more concerning is that the TPA and the free-carrier relaxation are inevitably accompanied by lattice heating,[32] which in turn contributes to the optical modulation via the thermo-optic effect. This contribution is long-lived, because the cooling of the lattice is governed by slow phonon−phonon scattering processes that have nanosecond relaxation times, resulting in an inherent limitation to the switching speed of nanoscale silicon resonators for nonlinear nanophotonics. It is worth pointing out that this limitation is not restricted to silicon-based nanostructures: it is also present in plasmonic nanoparticles and metasurfaces, where the all-optical modulation is achieved by exploiting a thermo-modulational nonlinearity (see, e.g., refs 33, 34). Here, we present an avenue to overcome such limitations and then demonstrate ultrafast all-optical transmission modulation in a-Si:H with full recovery on the picosecond time scale. Our approach starts from the experimental and theoretical analyses of the large optical nonlinearity exhibited by a-Si:H metasurfaces with anisotropic meta-atoms across the whole visible spectrum. Such a combined study enables us to disentangle the physical mechanisms governing the observed nonlinearity, and quantitatively elucidates the contribution of each to the transient modulation of the anisotropic Mie-like resonances. This allows us to identify the avenue by which the contribution arising from the slow processes that limit modulation speed can be suppressed at selected wavelengths within a given resonance or even in-between two neighboring resonances thanks to competing effects. These results offer a new premise for exploiting all-dielectric metasurfaces for ultrafast spectral and polarization switching.

EXPERIMENTS AND MODELING

A two-dimensional array of a-Si:H nanobricks was manufactured by lithography on a thin a-Si:H film of thickness d = 175 nm, which was grown on a silica substrate with plasma-enhanced chemical vapor deposition (see Methods). A scanning electronic microscopic (SEM) image of the a-Si:H metasurface is shown in Figure 1a. The linear optical response at normal incidence was investigated both experimentally and numerically (cf. Figure 1b), and the results are reported in Figure 1c and d. Note that the anisotropic shape of the meta-atom results in a highly anisotropic optical response, with a dominant resonance at 650 nm for the X-polarization (X-pol) and two resonances located at 600 and 750 nm for the Y-polarization (Y-pol). The numerical simulations were performed with full-wave finite element software (CST Microwave Studio) using the measured complex permittivity of a-Si:H obtained from the initial 175 nm film of a-Si:H and are in good agreement with the experimental data.

We investigate the transient optical response of the a-Si:H metasurface with broadband polarization-resolved pump−probe spectroscopy. Importantly, the a-Si:H offers much faster relaxation of free carriers in comparison to crystalline semiconductors,[31,32] hence the possibility for faster optical modulation. Our experimental setup is based on an amplified Ti:sapphire laser (Coherent, Libra) producing 100 fs pulses at 800 nm wavelength. The sample was excited either by the laser fundamental wavelength at 800 nm or by its second harmonic at 400 nm, i.e., at the two extrema of the spectral range of interest in our investigation (Figure 1d), so as to avoid pump−probe degeneracy artifacts at the Mie resonances. Moreover, these two wavelengths are at the two extrema also with respect to the absorption regimes, the latter being dominated by linear absorption, the former by a nonlinear one (Figure 2c,d). This allows us to provide a clear-cut disentanglement of the two regimes of pump excitation (see below). The probe pulse was obtained by supercontinuum generation, starting from a fraction of the laser beam (see Supporting Information for further details).

We measure the differential transmission ($\Delta T/T$), defined as the difference between the transmitted light spectra at normal incidence with and without the pump, normalized to the transmitted light spectrum without the pump.

We finally develop a theoretical model for the optical nonlinearity. When a pump pulse of intensity $I(t)$ impinges on the a-Si:H metasurface, free carriers (electrons in the conduction band and holes in the valence band) are generated, at a rate $\Phi(t)$ per unit volume, by either linear or nonlinear absorption processes, as sketched in Figure 2a (left panel). Given a-Si:H is an indirect band gap semiconductor with an energy gap of about 1.7 eV, the free carrier volume density N relaxes nonradiatively by means of a first-order trap-assisted process, with characteristic time $\tau_{tr} \simeq 30$ ps,[30] or via second-order bimolecular recombination at a rate $\gamma = 2.3 \times 10^{-8}$ cm^3/s.[35,36] In order to conserve the energy, each relaxation event occurs alongside phonon generation, which contributes to lattice heating with an energy equal to that of the electron−hole pair.[32] This causes an increase of the lattice temperature Θ with respect to the ambient temperature Θ_a. The dynamical properties of the a-Si:H metasurface are thus governed by three variables: the pump pulse incident intensity $I(t)$, the free-carrier density $N(t)$, and the lattice temperature $\Theta(t)$. Each of

DOI: 10.1021/acsphotonics.7b00544
ACS Photonics 2017, 4, 2129−2136

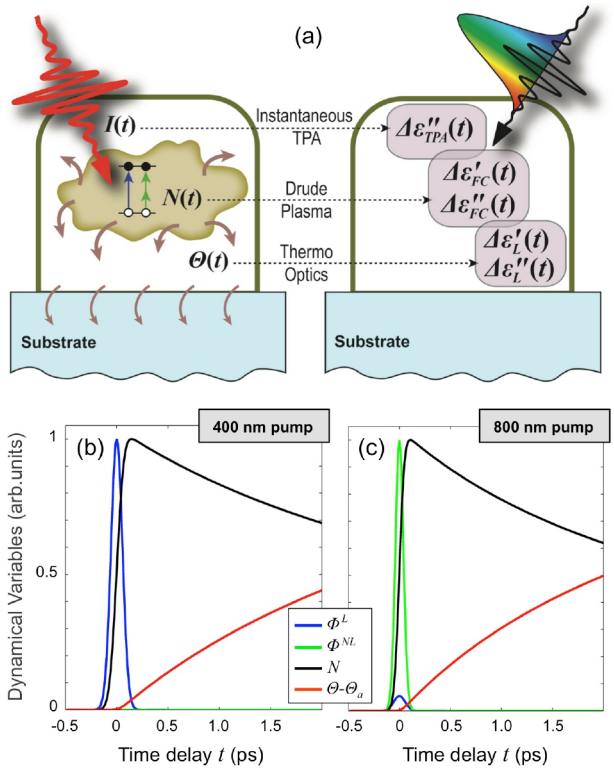

Figure 2. (a) Illustration of the nonlinear optical processes in the a-Si:H meta-atom. The interaction with a monochromatic pump beam (left panel) gives rise to a modification of the a-Si:H permittivity experienced by the broadband probe pulse (right panel), according to three different physical mechanisms: instantaneous TPA, Drude plasma response, and thermo-optical effect. (b, c) Dynamics of the linear $\Phi^{L}(t)$ and nonlinear $\Phi^{NL}(t)$ drives and of the solution, $N(t)$ and $\Theta(t)$, of the rate equation model governing the nonlinear optical processes. Results for *Y*-pol pump wavelength excitation at (b) 400 nm and (c) 800 nm are compared.

these variables then presides over a different mechanism responsible for the pump-induced variation $\Delta\epsilon$ of the complex permittivity experienced by a weak probe pulse of wavelength λ, arriving on the metasurface at a time delay t with respect to the pump. This is illustrated in the right panel of Figure 2a: the intensity $I(t)$ translates into a purely imaginary instantaneous $\Delta\epsilon_{TPA}$ via TPA; the free-carrier density $N(t)$ is responsible for a transient Drude plasma permittivity $\Delta\epsilon_{FC}$, having both real and imaginary parts; finally, the lattice temperature $\Theta(t)$ induces a thermo-optic modulation $\Delta\epsilon_{L}$. Note that the dominant free-carrier generation mechanism is linear absorption above the band gap and nonlinear absorption below the band gap. Our three variables are also coupled together by a system of rate equations (see Methods), whose typical evolutions are illustrated in Figure 2b and c for pump wavelengths above and below the band gap, 400 and 800 nm, respectively. One observes, following linear (nonlinear) free-carrier generation, their recombination on the picosecond time scale, which leads to an increase of the lattice temperature.

It should be noted that the present model, being grounded on a rate-equation formalism, disregards coherent effects of light−matter interaction in the nonlinear optical response. This is based on the assumption that the laser pulse duration (100 fs) is much longer than the dephasing time of the system. Actually, noncrystalline semiconductor materials, e.g., porous silicon[37] or glasses doped with semiconductor microcrystals,[38] are known to exhibit a dephasing time on the order of few tens of fs or even less, because of the high carrier scattering rates induced by defects and surface states. Even though a specific study on the subject is missing, we assumed the same behavior in a-Si:H nanobricks, in accord with ref 30.

With the dynamic transient permittivity $\Delta\epsilon$ at hand, the transient optical transmission spectrum of the metasurface as a function of both λ and t can be calculated as a perturbation of the previous full-wave numerical simulations of the linear system (see Methods).

RESULTS

The experimental $\Delta T/T$ maps under a Y-pol pump at 400 nm wavelength and the dynamics at selected probe wavelengths are reported in Figure 3a and c for X-pol and Y-pol probe, respectively. Following a pulse-width-limited build-up, the $\Delta T/T$ signal decays on the time scale of a few ps, which is much longer than the pulse duration (~100 fs). The initial $\Delta T/T$ spectra are dominated by blue-shifts of the three Mie-like resonances observed in the linear optical response (cf. Figure 1c), but the scenario then evolves with time. Eventually there can be a sign reversal of $\Delta T/T$, corresponding to a red-shift at long time delays, such as seen in the dynamics of the Y-pol probe at 645 nm wavelength (green curve in the bottom panel of Figure 3a). This is a clear indication that the signal is now not due to TPA but rather to the free carriers and hot lattice contributions. However, for different wavelengths, such as the orange curves in the bottom panels of Figure 3c,d, the signal can instead monotonically increase from zero toward a long-lasting plateau within a few ps. All these features are further accurately reproduced by our model, as detailed by the simulated maps and temporal cross sections of Figure 3b and d. It is worth recognizing that the anisotropy of this transient behavior, such as seen in Figure 3a,b vs c,d, can generally allow one to tune the angle of polarization in transmission. By utilizing slightly detuned resonances between axes, the X- and Y-pols can experience opposite changes to absolute transmission and thereby provide mutually constructive polarization rotation. A similar conclusion could also be made for reflection, given absorption of the probe is negligible.

A different scenario is then observed when pumping in the near infrared. The experimental $\Delta T/T$ map for a Y-pol probe under Y-pol pumping at 800 nm is shown in the top panel of Figure 4a, together with time traces at selected probe wavelengths (bottom panel). The instantaneous contribution to the transient optical response due to TPA is now very prominent, such as seen in the orange and green traces in the bottom panel of Figure 4a. This behavior is accurately reproduced by the model, as seen in Figure 4b, and is observed also in the $\Delta T/T$ map for a X-pol probe, not shown here (see Supporting Information).

No dependence on pump polarization is observed in the transient optical response of the metasurface (as detailed in the Supporting Information), apart from a uniform change in the absolute value of the signal, corresponding to the difference in the anisotropic linear absorption of the pump pulse (cf. dotted lines in Figure 1d). Hence only the two probe polarizations are relevant.

The presented theoretical model is able to quantitatively reproduce the complete transient response for both probe polarizations across our broad spectrum, while employing only *two* fixed fitting parameters: (i) the effective TPA coefficient β_{TPA}^{eff} and (ii) the κ parameter of the imaginary thermo-optic

DOI: 10.1021/acsphotonics.7b00544
ACS Photonics 2017, 4, 2129−2136

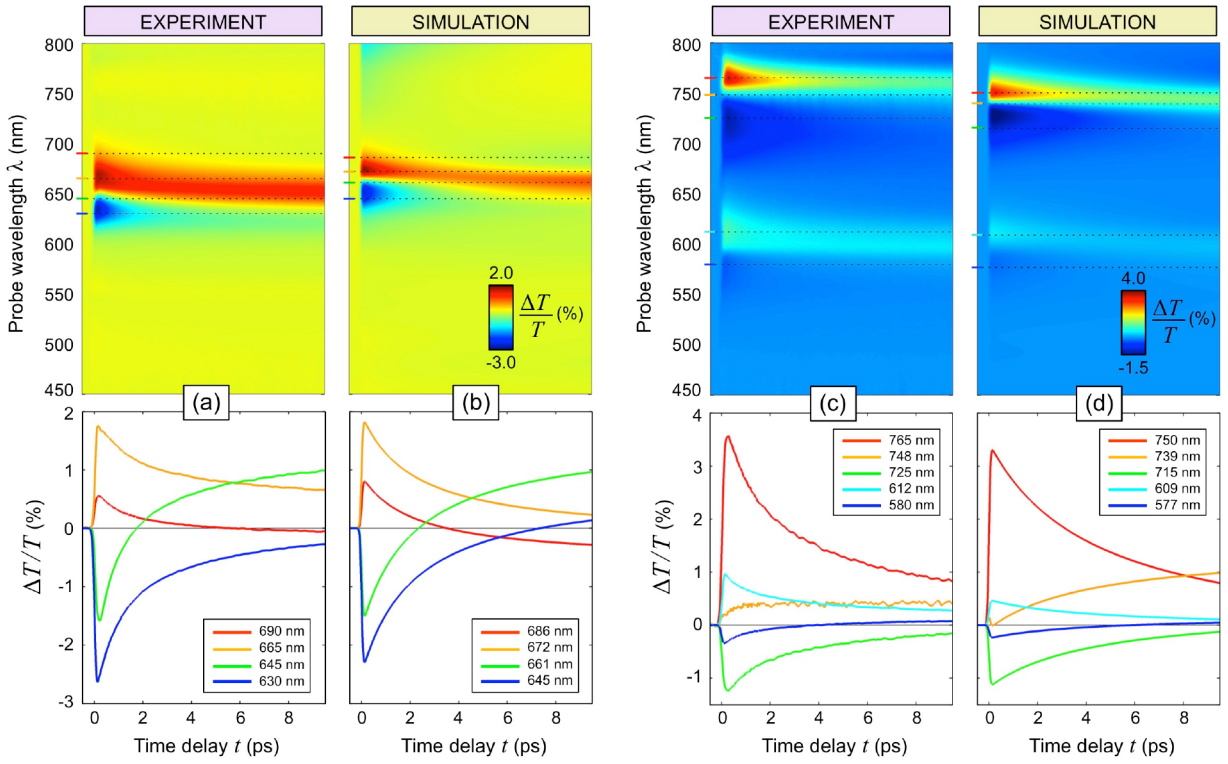

Figure 3. Polarization-resolved relative differential transmission under Y-pol pumping with a Gaussian pulse of duration $\tau_p \simeq 110$ fs and fluence $F \approx 0.1$ mJ/cm^2 at 400 nm wavelength. (a) Measurement ($F = 105$ μJ/cm^2) versus (b) simulation ($F = 121$ μJ/cm^2), for X-pol probe. (c) Measurement ($F = 83$ μJ/cm^2) versus (d) simulation ($F = 59$ μW/cm^2) for Y-pol probe. Top panels show the $\Delta T/T$ maps as a function of time delay t and probe wavelength λ. Bottom panels show map cross sections at some selected wavelengths, corresponding to the dotted lines in the top panels.

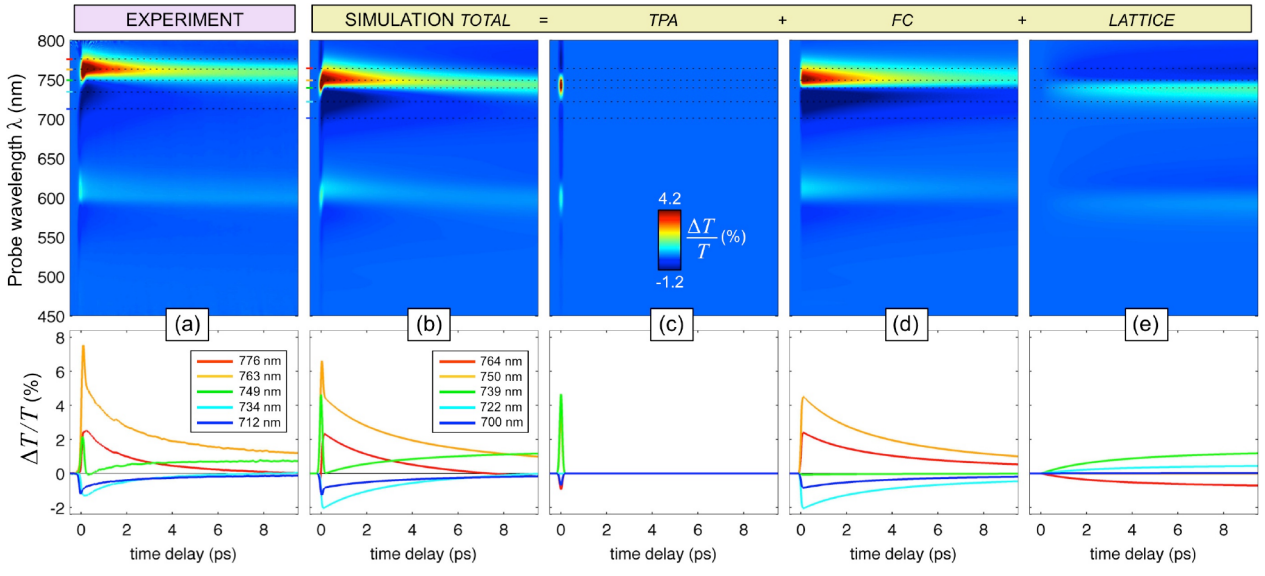

Figure 4. Relative differential transmission under Y-pol pumping at 800 nm and Y-pol broadband probing: (a) Measurement ($F = 0.8$ mJ/cm^2) versus (b) simulation ($F = 1$ mJ/cm^2). Panels (c)−(e) show the three different contributions to the total simulated map of panel (b) given by the instantaneous TPA, the free carriers, and the lattice. Top panels show the $\Delta T/T$ maps as a function of time delay t and probe wavelength λ (with 50% colormap saturation for better reading). Bottom panels show map cross sections at selected wavelengths, corresponding to the dotted lines in the top panels.

coefficient (defined in the Methods). A fitting procedure retrieves $\beta_{TPA}^{eff} = 0.15$ cm/MW, which is about 3 times higher than the value reported in a-Si:H thin films of comparable thickness, suggesting that the nanostructuring enhances the nonlinear response despite the reduction of the filling factor of the nonlinear medium. The retrieved thermo-optic coefficient was found to be $\kappa = 80$ K^{-1} cm^{-1}. Considering the substantial dispersion of values reported in the literature, depending on wavelength (about 2 orders of magnitude increase from 750 nm to 650 nm) and on the exact composition and structure of the a-Si:H amorphous matrix, the value retrieved by our fit is in line with expectations (see, e.g., refs 39, 40 and references therein).

DOI: 10.1021/acsphotonics.7b00544
ACS Photonics 2017, 4, 2129−2136

It is worth pointing out that both the fitting parameters are effective parameters of the considered a-Si:H metasurface, depending on the bulk properties of a-Si:H and on the actual distribution of the electromagnetic fields in the nanobricks.

Given this theoretical model is able to correctly reproduce experiment, it can now be exploited to elucidate the origin of the spectral and temporal features observed in the experimental $\Delta T/T$ maps. We separate the contributions from each of the three different nonlinear mechanisms taking place under pumping in the near infrared (800 nm), i.e., the instantaneous TPA (Figure 4c), the Drude plasma response from optically generated free carriers (Figure 4d), and the thermo-optic effect arising from lattice heating (Figure 4e). This decomposition confirms that the observed noninstantaneous processes are indeed caused by free carriers and lattice heating. However, free carriers induce a blue shift of the resonances (Figure 4d), whereas lattice heating is associated with a red shift (Figure 4e). These two mechanisms can thus partially compensate each other within an individual resonance until the free-carrier relaxation is completed. On the contrary, the instantaneous TPA (Figure 4c) causes an increase of transmission at around the peak of the resonances (600 and 750 nm) and a decrease at the sides of these peaks, meaning that TPA results in an instantaneous broadening of the resonances. This explains the peculiar dynamics observed experimentally at around 749 nm (green curve in the bottom panel of Figure 4a) and in the simulations at around 739 nm (the 10 nm blue shift is due to the small shift in the linear spectra of Figure 1d and c), where the ultrafast initial peak is followed by the buildup, on the picosecond time scale, of a long-living plateau. This behavior is due to a complete suppression of the contribution arising from the free carriers, providing zero $\Delta T/T$ at this wavelength, as detailed by the green curve in Figure 4d. Similarly, the orange traces and the blue traces in the bottom panels of Figure 4 correspond to signal wavelengths where the lattice contribution is suppressed in the total $\Delta T/T$, having zero value in the disentangled traces of Figure 4e.

The suppression of the contribution from the slowest processes taking place in the transient nonlinear optical response of a-Si:H metasurfaces is of major relevance in view of ultrafast all-optical switching applications. The disentanglement procedure detailed above can be utilized to identify all the wavelength ranges, or operating bands, where such suppression is obtained. Figure 5 shows the absolute value of the simulated differential transmission $|\Delta T|$ as a function of the probe wavelength [Y-pol probe in panel (a) and X-pol probe in panel (b)], arising from the three different contributions to the optical nonlinearity, each one evaluated at the time delay where the corresponding dynamical variable, either $I(t)$, $N(t)$, or $\Theta(t)$, achieves its maximum (cf. Figure 2). Thanks to the peculiar differences between the three physical mechanisms of the all-optical modulation pointed out above, the maximum of the instantaneous $|\Delta T|$ due to TPA (blue curve) is achieved close to those wavelengths where the noninstantaneous contributions, either from the free carriers (green) or from the lattice (red), approach a negligible value and eventually nullify. To provide a quantitative estimation of this effect, we introduce a figure of merit defined as the polarization-dependent rejection ratio $RR_{X(Y)} = 10\ \log_{10}(|\Delta T^{ins}_{X(Y)}|/|\Delta T^{del}_{X(Y)}|)$, where ΔT^{ins} is the differential transmission due to instantaneous TPA at zero time delay (blue curves in Figure 5), and ΔT^{del} is the differential transmission from delayed nonlinear processes, i.e., due to either the free carriers (at 0.1 ps time delay) or the lattice heating (at about 20 ps time delay, when the free-carrier dynamics are exhausted).

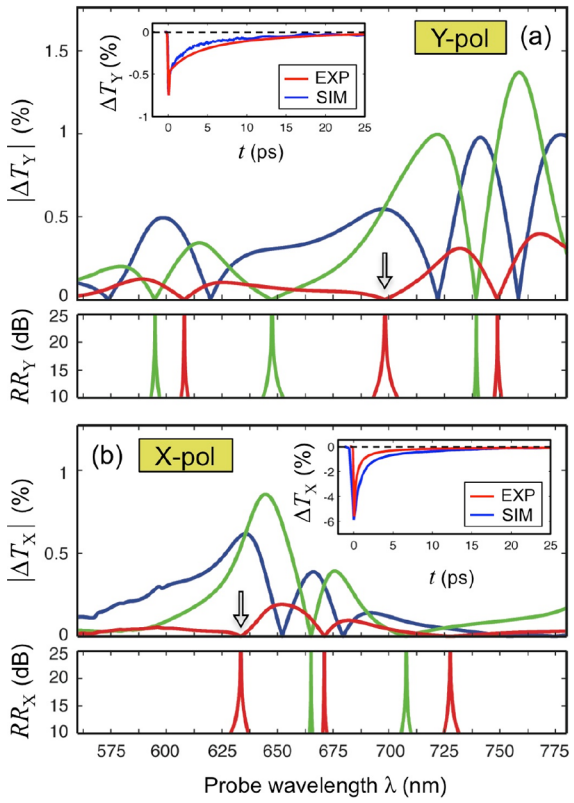

Figure 5. High-speed modulation windows. (a) Differential transmission spectra (in modulus) for Y-pol probe (pump fluence F = 0.8 mJ/cm^2), arising from the instantaneous TPA at t = 0 ps (blue), the free carriers at $t \simeq 0.1$ ps (green), and the lattice at $t \simeq 20$ ps (red). Bottom panel shows the modulation windows with high rejection of the free-carriers (green) and lattice (red) contributions. Inset shows the experimental $\Delta T_Y(t)$ on a time scale of 25 ps, evaluated at 713 nm, compared with the experimental $\Delta T_Y(t)$ at 700 nm (operating band pointed out by arrow). (b) Same as (a) but for X-pol probe and pump fluence F = 1.1 mJ/cm^2. Insets show the experimental and simulated $\Delta T_X(t)$ on a time scale of 25 ps, evaluated at around 630 nm (arrow in the main graph) but with F = 2 mJ/cm^2.

By plotting the values of $RR_{Y(X)}$ exceeding a given threshold, chosen here at 10 dB, it is possible to identify suitable operation windows where the signal modulation is almost unaffected by either the free-carrier Drude response (green curves in the bottom panels of Figure 5a and b) or the thermo-optic effect related to the lattice heating (red curves in the bottom panel of Figure 5a and b). Most interestingly, the latter operating bands provide a full return to zero differential signal upon relaxation of the optically generated free carriers. This is confirmed by the experimental ΔT traces reported in the inset of Figure 5 for the operating bands pointed out by arrows in the main graphs. It is worth recognizing that this is possible despite the fact that the thermal contribution is very long-lasting, taking place on the nanosecond time scale. Among these different operating bands with a full return to zero, the one located at around 700 nm for the Y-pol probe is particularly interesting for two reasons: (i) the operating band is comparatively broad in-between the resonances (cf. Figure 1c,d); (ii) the linear transmission is much higher, implying larger absolute modulation of transmission from TPA, while also enabling the possibility for cascaded operation through consecutive surfaces, due to low

DOI: 10.1021/acsphotonics.7b00544
ACS Photonics 2017, 4, 2129−2136

reflection losses. The dynamics of this operating band can then be elucidated by looking at the different transmission modulation mechanisms illustrated in Figure 4. In-between the two Mie-like resonances at 700 nm, the contributions from instantaneous TPA (Figure 4c) superimpose constructively, whereas the contributions from the lattice heating (Figure 4e) superimpose destructively.

DISCUSSION AND CONCLUSION

We have chosen to keep our study in a perturbative regime where the maximum $|\Delta T|$ is around 1% (cf. main graphs in Figure 5); however ΔT can easily be increased on the order of 10% by increasing the pump fluence from 1.1 to 2 mJ/cm^2, as demonstrated in the inset of Figure 5b. This was performed when pumping in the near infrared, where the TPA nonlinearity dominates both the instantaneous contribution and as the source of nonlinear free-carrier generation (cf. Figure 2c). Note that the increase of fluence accelerates the recovery of the signal due to a faster relaxation of the free carriers induced by a higher bimolecular recombination rate (which is nonlinear in the free-carrier concentration), thus approaching the carrier relaxation time of about 10 ps typical of plasmonic nanoparticles (see, e.g., ref 41). Moreover, fresh results from other all-dielectric nanostructures (GaAs nanoparticles) indicate that carrier relaxation mediated by surface states can further speed up the recovery time to a few ps.[23] Despite our model being perturbative, a preliminary estimation of the pump fluence required to achieve a full modulation of the transmittance (i.e., $|\Delta T| \approx |T|$), combined with a sizable transmission in the linear regime, is on the order of 3−4 mJ/cm^2. This value is compatible with the damage threshold of our metasurface, according to the estimation given in ref 30 (and supported further by the lower $\beta_{\mathrm{TPA}}^{\mathrm{eff}}$, and thus lower free-carrier generation and thermal load, of the present configuration), and turns out to be in line with state-of-the-art all-optical modulation performance from plasmonic metasurfaces.[6,7]

In light of the results presented above, we can now outline two further developments for nonlinear anisotropic a-Si:H metasurfaces:

1. When the probe is linearly polarized at an angle α with respect to the X-axis, it will experience a modulation given by $\Delta T_\alpha = \cos^2(\alpha)\Delta T_X + \sin^2(\alpha)\Delta T_Y$. Using our theoretical model (see Methods), the free-carrier and lattice heating contributions to ΔT_X and ΔT_Y are respectively then linearly proportional to the same free carrier density N or lattice temperature Θ. Subsequently, at any probe wavelength, where ΔT_X and ΔT_Y have opposite sign, there is guaranteed to be a polarization angle α where the free carrier or lattice heating contribution toward ΔT_α can be made precisely zero, independent of the respective N or Θ. This suggests that the high-speed modulation windows can be easily tuned by simply rotating the metasurface. One could even design an optimized metasurface where, for a particular value of α, simultaneous suppression of contributions from both lattice heating and free carriers is made possible, meaning the recovery to zero of the differential signal ceases to be limited by material response.

2. The nonlinear anisotropy of the nanobrick resonators should provide modulation of the phase and amplitude mismatch between the X-pol and Y-pol field components. Modulated amplitude mismatch then provides polarization rotation, while phase mismatch provides waveplate transformations. This suggests that such a metasurface could operate as an ultrafast new type of all-optical, dynamical wave plate in a flat-optics configuration.

In conclusion, the presented broadband polarization-resolved pump−probe experiments have revealed a complex scenario for the transient optical response of anisotropic a-Si:H metasurfaces excited by intense femtosecond laser pulses. We have introduced a quantitative model for the observed optical nonlinearity spanning the whole visible spectrum and validated by the experimental data. This allowed us to disentangle the different physical mechanisms presiding over the all-optical modulation capability of the a-Si:H metasurface. It was found that, despite the onset of dynamical processes in the a-Si:H material that included very slow thermal effects, a sizable modulation of light transmittance with a full recovery to zero within about 20 ps is achievable in a range of operation windows. Furthermore, the observed ultrafast dynamics can be multiplexed in polarization due to the anisotropy of the metasurface. Our results hence pave the way to the engineering of novel all-dielectric nonlinear metamaterials based on a-Si:H nanostructures, enabling a next generation of ultrafast all-optical nanophotonic devices, including optical switches and polarization rotators.

METHODS

Sample Fabrication. Arrays of silicon nanobricks were fabricated by electron beam lithography on a polycrystalline silicon film deposited on a glass substrate via PECVD technique. The substrate was coated with ZEP (a positive-tone electron-beam resist) and baked at 180 °C for 120 s. Patterns of silicon bricks were then defined by an electron beam exposure, followed by a development procedure. Subsequently, a 10 nm thick Cr film was deposited by thermal evaporation on the substrate, followed by lift-off. The structures were then transferred to the silicon substrates via a reactive ion etch using the Cr bar nanostructures as etch masks. The residual Cr was then removed via wet etching to obtain the pure Si nanobricks.

Nonlinear Model of a-Si:H Metasurfaces. The optically induced dynamical processes taking place in the a-Si:H metaatoms are quantitatively modeled by the following rate equations:

$$\dot{N}(t) = -\left(\gamma N(t) + \frac{1}{\tau_{\mathrm{tr}}}\right)N(t) + \Phi(t) \tag{1}$$

$$C\dot{\Theta}(t) = E_{\mathrm{eh}}\left(\gamma N(t) + \frac{1}{\tau_{\mathrm{tr}}}\right)N(t) \tag{2}$$

In the above equations, E_{eh} is the energy of the electron−hole pair, equal to $h\nu_p$ for linear absorption or $2h\nu_p$ for TPA, C = 1.66 J K^{-1} cm^{-3} is the a-Si:H volume-specific heat, which is assumed to be equal to that of silicon,[30] and $\Phi(t)$ is the free-carrier generation rate per unit volume that drives the system. The latter is the sum of two contributions, one from linear absorption and one from nonlinear TPA, respectively given by $\Phi^{\mathrm{L}}(t) = 1/(h\nu_p)A_{\mathrm{L}}I(t)S/V$ and $\Phi^{\mathrm{NL}}(t) = 1/(2h\nu_p)A_{\mathrm{NL}}(I)I(t)S/V$, with ν_p being the frequency of the pump laser pulse with intensity $I(t)$, S the area of the unit cell of the metasurface, V the volume of the metaatom, and A_{L} (A_{NL}) the linear (nonlinear) absorption of the metasurface. The linear absorption A_{L} for both X-pol and Y-pol is retrieved from full-wave finite element numerical analysis (cf. Figure 1d). For

DOI: 10.1021/acsphotonics.7b00544
ACS Photonics 2017, 4, 2129−2136

the nonlinear absorption we assumed the simple isotropic expression $A_{NL}(I) = 1 - \exp[-\beta_{TPA}^{eff} I(t) d]$.

The above equation system is numerically solved for a Gaussian pulse of intensity $I(t) = I_0 \exp(-2t^2/\tau_p^2)$ with $I_0 = F/(\tau_p\sqrt{\pi/2})$, F and τ_p being the incident fluence and the pulse duration, respectively.

The pump incident intensity I is responsible, via TPA, for an instantaneous and dispersionless (i.e., λ-independent) variation of the absorption coefficient α of a-Si:H given by $\Delta\alpha(t) = \beta_{TPA}^{eff} I(t)$. This corresponds to an instantaneous imaginary change of the permittivity $\Delta\epsilon_{TPA}(t) = ic n'(\nu_p)/(2\pi\nu_p)\Delta\alpha(t)$, where c is the speed of light in a vacuum and $n'(\nu_p)$ is the real part of the refractive index of the unperturbed a-Si:H evaluated at the pump frequency.

The optically generated free carriers act as a plasma of density N, thus providing a permittivity variation $\Delta\epsilon_{FC}(\lambda, t) = \Delta\epsilon'_{FC}(\lambda, t) + i\Delta\epsilon''_{FC}(\lambda, t)$ given by the Drude formulas

$$\Delta\epsilon'_{FC}(\lambda, t) = -\frac{N(t)e^2}{m^*\epsilon_0(4\pi^2c^2\lambda^{-2} + \tau_d^{-2})} \tag{3}$$

$$\Delta\epsilon''_{FC}(\lambda, t) = -\frac{\lambda\Delta\epsilon'_{FC}(\lambda, t)}{2\pi c\tau_d} \tag{4}$$

where ϵ_0 is the vacuum permittivity, $m = 0.12m_0$ with m_0 being the free electron mass, and $\tau_d = 0.8$ fs is the Drude damping time (in agreement with ref 30).

Finally, the lattice temperature variation $\Delta\Theta(t) = \Theta(t) - \Theta_a$ gives rise, via a thermo-optic effect, to a permittivity modulation $\Delta\epsilon_L(\lambda, t) = \Delta\epsilon'_L(\lambda, t) + i\Delta\epsilon''_L(\lambda, t)$ given by

$$\Delta\epsilon'_L(\lambda, t) = 2[n'(\lambda)\eta_1 - n''(\lambda)\eta_2]\Delta\Theta(t) \tag{5}$$

$$\Delta\epsilon''_L(\lambda, t) = 2[n''(\lambda)\eta_1 + n'(\lambda)\eta_2]\Delta\Theta(t) \tag{6}$$

where $n(\lambda) = n'(\lambda) + in''(\lambda)$ is the complex refractive index of the unperturbed a-Si:H evaluated at the probe wavelength, and $\eta_1 = dn'/d\Theta$ and $\eta_2 = dn''/d\Theta = \kappa\lambda/(4\pi)$ are the thermo-optic coefficients of a-Si:H. We assumed $\eta_1 = 4.5 \times 10^{-4}$ K^{-1} (in agreement with refs 30, 35) and $\kappa = 80$ K^{-1} cm^{-1} (fitted on the pump–probe experimental data).

The total $\Delta\epsilon(\lambda, t) = \Delta\epsilon'(\lambda, t) + i\Delta\epsilon''(\lambda, t)$ arising from the superposition of all the different contributions detailed above is employed to compute the temporal variation of the transmittance spectrum of the optically excited metasurface, $\Delta T(\lambda, t)$, against the transmittance spectrum $T(\lambda)$ of the unperturbed one. This is done perturbatively according to the formula

$$\Delta T(\lambda, t) = \psi(\lambda; \text{pol})\,\Delta\epsilon'(\lambda, t) + \phi(\lambda; \text{pol})\,\Delta\epsilon''(\lambda, t) \tag{7}$$

where the polarization-dependent spectral coefficients $\psi(\lambda; \text{pol})$ and $\phi(\lambda; \text{pol})$ are given by numerical computation of respectively the derivatives $dT/d\epsilon'$ and $dT/d\epsilon''$, evaluated at the probe wavelength. The ψ and ϕ spectral coefficients (shown in the Supporting Information) are strongly dispersive and turned out to be dominated by resonant features that belong to the Mie resonances of the linear spectra (cf. Figure S2b,c and Figure 1d). Therefore, by acting on the size and shape of the meta-atom the ψ and ϕ coefficients can be easily controlled, thus enabling a wavelength tuning of the nonlinear optical response, including, in principle, a coarse wavelength scaling of the ultrafast modulation windows with full return to zero.

■ ASSOCIATED CONTENT

Supporting Information

The Supporting Information is available free of charge on the ACS Publications website at DOI: 10.1021/acsphotonics.7b00544.

Additional information (PDF)

■ AUTHOR INFORMATION

Corresponding Authors

*E-mail: giuseppe.dellavalle@polimi.it.

*E-mail: Dragomir.Neshev@anu.edu.au.

ORCID

Giuseppe Della Valle: 0000-0003-0117-2683

Ben Hopkins: 0000-0002-4570-4269

Dragomir N. Neshev: 0000-0002-4508-8646

Notes

The authors declare no competing financial interest.

■ ACKNOWLEDGMENTS

The authors acknowledge support by the Australian Research Council and participation in the Erasmus Mundus NANOPHI project (contract number 2013 5659/002-001). G.C. acknowledges support from the European Union Horizon 2020 Programme under grant agreement no. 696656. G.D.V. acknowledges support by the Italian MIUR through the PRIN 2015 grant no. 2015WTW7J3. We thank M. R. Shcherbakov, A. E. Miroshnichenko, and L. Carletti for useful discussions. The authors acknowledge the use of the Australian National Fabrication Facility (ANFF), the ACT Node.

■ REFERENCES

(1) Kildishev, A. V.; Boltasseva, A.; Shalaev, V. M. Planar Photonics with Metasurfaces. *Science* **2013**, *339*, 1289.

(2) Yu, N.; Capasso, F. Flat optics with designer metasurfaces. *Nat. Mater.* **2014**, *13*, 139.

(3) Li, G.; Zhang, S.; Zentgraf, T. Nonlinear photonic metasurfaces. *Nature Reviews Materials* **2017**, *2*, 17010.

(4) Sun, C.-K.; Vallée, F.; Acioli, L. H.; Ippen, E. P.; Fujimoto, J. G. Femtosecond-tunable measurement of electron thermalization in gold. *Phys. Rev. B: Condens. Matter Mater. Phys.* **1994**, *50*, 15337–15348.

(5) Boyd, R. W.; Shi, Z.; Leon, I. D. The third-order nonlinear optical susceptibility of gold. *Opt. Commun.* **2014**, *326*, 74–79.

(6) Wurtz, G. A.; Pollard, R.; Hendren, W.; Wiederrecht, G. P.; Gosztola, D. J.; Podolskiy, V. A.; Zayats, A. V. Designed ultrafast optical nonlinearity in a plasmonic nanorod metamaterial enhanced by nonlocality. *Nat. Nanotechnol.* **2011**, *6*, 107–111.

(7) Kauranen, M.; Zayats, A. V. Nonlinear plasmonics. *Nat. Photonics* **2012**, *6*, 737–748.

(8) Baida, H.; Mongin, D.; Christofilos, D.; Bachelier, G.; Crut, A.; Maioli, P.; Del Fatti, N.; Vallée, F. Ultrafast Nonlinear Optical Response of a Single Gold Nanorod near Its Surface Plasmon Resonance. *Phys. Rev. Lett.* **2012**, *107*, 1–5.

(9) Brinks, D.; Castro-Lopez, M.; Hildner, R.; van Hulst, N. F. Plasmonic antennas as design elements for coherent ultrafast nanophotonics. *Proc. Natl. Acad. Sci. U. S. A.* **2013**, *110*, 18386–18390.

(10) Zavelani-Rossi, M.; Polli, D.; Kochtcheev, S.; Baudrion, A.-L.; Beal, J.; Kumar, V.; Molotokaite, E.; Marangoni, M.; Longhi, S.; Cerullo, G.; Adam, P.-M.; Della Valle, G. Transient Optical Response of a Single Gold Nanoantenna: The Role of Plasmon Detuning. *ACS Photonics* **2015**, *2*, 521–529.

DOI: 10.1021/acsphotonics.7b00544
ACS Photonics 2017, 4, 2129–2136

(11) Wang, X.; Morea, R.; Gonzalo, J.; Palpant, B. Coupling Localized Plasmonic and Photonic Modes Tailors and Boosts Ultrafast Light Modulation by Gold Nanoparticles. *Nano Lett.* **2015**, *15*, 2633−2639.
(12) Harutyunyan, H.; Martinson, A. B. F.; Rosenmann, D.; Khorashad, L. K.; Besteiro, L. V.; Govorov, A. O.; Wiederrecht, G. P. Anomalous ultrafast dynamics of hot plasmonic electrons in nanostructures with hot spots. *Nat. Nanotechnol.* **2015**, *10*, 770−774.
(13) Faggiani, R.; Losquin, A.; Yang, J.; MÅrsell, E.; Mikkelsen, A.; Lalanne, P. Modal Analysis of the Ultrafast Dynamics of Optical Nanoresonators. *ACS Photonics* **2017**, *4*, 897−904.
(14) Ciappina, M. F.; et al. Attosecond physics at the nanoscale. *Rep. Prog. Phys.* **2017**, *80*, 054401-1−054401-50.
(15) Stockman, M. I. Ultrafast nanoplasmonics under coherent control. *New J. Phys.* **2008**, *10*, 025031-1−025031-20.
(16) Khurgin, J. B.; Boltasseva, A. How to deal with the loss in plasmonics and metamaterials. *MRS Bull.* **2012**, *37*, 768−779.
(17) Naik, G. V.; Shalaev, V. M.; Boltasseva, A. Alternative Plasmonic Materials: Beyond Gold and Silver. *Adv. Mater.* **2013**, *25*, 3264−3294.
(18) Boltasseva, A.; Atwater, H. A. Ultrafast Active Plasmonics. *Science* **2011**, *331*, 290−291.
(19) Comin, A.; Manna, L. New materials for tunable plasmonic colloidal nanocrystals. *Chem. Soc. Rev.* **2014**, *43*, 3957−3975.
(20) Scotognella, F.; Della Valle, G.; Kandada, A. R. S.; Zavelani-Rossi, M.; Longhi, S.; Lanzani, G.; Tassone, F. Plasmonics in heavily-doped semiconductor nanocrystals. *Eur. Phys. J. B* **2013**, *86*, 1−13.
(21) Koppens, F. H.; Chang, D. E.; Garcia de Abajo, F. J. Graphene plasmonics: a platform for strong light-matter interactions. *Nano Lett.* **2011**, *11*, 3370−3377.
(22) Kuznetsov, A. I.; Miroshnichenko, A. E.; Brongersma, M. L.; Kivshar, Y. S.; Lukyanchuk, B. Optically resonant dielectric nanostructures. *Science* **2016**, *354*, aag2472.
(23) Shcherbakov, M. R.; Liu, S.; Zubyuk, V. V.; Vaskin, A.; Vabishchevich, P. P.; Keeler, G.; Pertsch, T.; Dolgova, T. V.; Staude, I.; Brener, I.; Fedyanin, A. A. Ultrafast all-optical tuning of direct-gap semiconductor metasurfaces. *Nat. Commun.* **2017**, *8*, 17-1−7.
(24) Shcherbakov, M. R.; Neshev, D. N.; Hopkins, B.; Shorokhov, A. S.; Staude, I.; Melik-Gaykazyan, E. V.; Decker, M.; Ezhov, A. A.; Miroshnichenko, A. E.; Brener, I.; Fedyanin, A. A.; Kivshar, Y. S. Enhanced Third-Harmonic Generation in Silicon Nanoparticles Driven by Magnetic Response. *Nano Lett.* **2014**, *14*, 6488−6492.
(25) Yang, Y.; Wang, W.; Boulesbaa, A.; Kravchenko, I. I.; Briggs, D. P.; Puretzky, A.; Geohegan, D.; Valentine, J. Nonlinear Fano-Resonant Dielectric Metasurfaces. *Nano Lett.* **2015**, *15*, 7388−7393.
(26) Shorokhov, A. S.; Melik-Gaykazyan, E. V.; Smirnova, D. A.; Hopkins, B.; Chong, K. E.; Choi, D.- Y.; Shcherbakov, M. R.; Miroshnichenko, A. E.; Neshev, D. N.; Fedyanin, A. A.; Kivshar, Y. S. Multifold Enhancement of Third-Harmonic Generation in Dielectric Nanoparticles Driven by Magnetic Fano Resonances. *Nano Lett.* **2016**, *16*, 4857.
(27) Ikeda, K.; Shen, Y.; Fainman, Y. Enhanced optical nonlinearity in amorphous silicon and its application to waveguide devices. *Opt. Express* **2007**, *15*, 17761−17771.
(28) Sommer, A.; et al. Attosecond nonlinear polarization and light-matter energy transfer in solids. *Nature* **2016**, *534*, 86−90.
(29) Vampa, G.; Fattahi, H.; Vučković, J.; Krausz, F. Attosecond nanophotonics. *Nat. Photonics* **2017**, *11*, 201−212.
(30) Shcherbakov, M. R.; Vabishchevich, P. P.; Shorokhov, A. S.; Chong, K. E.; Choi, D.-Y.; Staude, I.; Miroshnichenko, A. E.; Neshev, D. N.; Fedyanin, A. A.; Kivshar, Y. S. Ultrafast All-Optical Switching with Magnetic Resonances in Nonlinear Dielectric Nanostructures. *Nano Lett.* **2015**, *15*, 6985−6990.
(31) Baranov, D. G.; Makarov, S. V.; Milichko, V. A.; Kudryashov, S. I.; Krasnok, A. E.; Belov, P. A. Nonlinear Transient Dynamics of Photoexcited Resonant Silicon Nanostructures. *ACS Photonics* **2016**, *3*, 1546−1551.
(32) Fauchet, P. M.; Hulin, D.; Vanderhaghen, R.; Mourchid, A.; W, N., Jr. The properties of free carriers in amorphous silicon. *J. Non-Cryst. Solids* **1992**, *141*, 76−87.
(33) Del Fatti, N.; Voisin, C.; Christofilos, D.; Vallée, F.; Flytzanis, C. Acoustic Vibration of Metal Films and Nanoparticles. *J. Phys. Chem. A* **2000**, *104*, 4321−4326.
(34) Hodak, J. H.; Henglein, A.; Hartland, G. V. Photophysics of Nanometer Sized Metal Particles: Electron-Phonon Coupling and Coherent Excitation of Breathing Vibrational Modes. *J. Phys. Chem. B* **2000**, *104*, 9954−9965.
(35) Fauchet, P. M.; Hulin, D. Ultrafast carrier relaxation in hydrogenated amorphous silicon. *J. Opt. Soc. Am. B* **1989**, *6*, 1024−1029.
(36) Esser, A.; Seibert, K.; Kurz, H.; Parsons, G. N.; Wang, C.; Davidson, B. N.; Lucovsky, G.; Nemanich, R. J. Ultrafast recombination and trapping in amorphous silicon. *Phys. Rev. B: Condens. Matter Mater. Phys.* **1990**, *41*, 2879−2884.
(37) Tomasiunas, R.; Moniatte, J.; Pelant, I.; Gilliot, P.; Hönerlage, B. Femtosecond dephasing in porous silicon. *Appl. Phys. Lett.* **1996**, *68*, 3296−3298.
(38) Huang, G. L.; Kwok, H. S. Femtosecond dephasing times in semiconductor microcrystals measured with incoherent light. *J. Opt. Soc. Am. B* **1992**, *9*, 2019−2024.
(39) Kovalev, D.; Polisski, G.; Ben-Chorin, M.; Diener, J.; Koch, F. The temperature dependence of the absorption coefficient of porous silicon. *J. Appl. Phys.* **1996**, *80*, 5978−5983.
(40) Poruba, A.; Springer, J.; Mullerova, L.; Beitlerova, A.; Vanecek, M.; Wyrsch, N.; Shah, A. Temperature dependence of the optical absorption coefficient of microcrystalline silicon. *J. Non-Cryst. Solids* **2004**, *338*−*340*, 222−227.
(41) Hodak, J.; Martini, I.; Hartland, G. V. Ultrafast study of electron-phonon coupling in colloidal gold particles. *Chem. Phys. Lett.* **1998**, *284*, 135−141.

DOI: 10.1021/acsphotonics.7b00544
ACS Photonics 2017, 4, 2129−2136